



RESEARCH ARTICLE

10.1029/2023JG007481

Key Points:

- We provide water chemistry data from 24 rivers with different watershed sizes in the Amur-Mid Basin during summer
- dFe and dissolved organic carbon concentrations showed a significant positive correlation with the coverage of the permafrost wetland in the watersheds
- Permafrost was confirmed underneath wetlands, and thickly accumulated peat soils were rich in organic matter

Supporting Information:

Supporting Information may be found in the online version of this article.

Correspondence to:

Y. Tashiro,
tassy40y@gmail.com

Citation:

Tashiro, Y., Yoh, M., Shesterkin, V. P., Shiraiwa, T., Onishi, T., & Naito, D. (2023). Permafrost wetlands are sources of dissolved iron and dissolved organic carbon to the Amur-Mid Rivers in summer. *Journal of Geophysical Research: Biogeosciences*, 128, e2023JG007481. <https://doi.org/10.1029/2023JG007481>

Received 20 MAR 2023

Accepted 1 AUG 2023

Author Contributions:

Conceptualization: Y. Tashiro
Data curation: Y. Tashiro, M. Yoh, V. P. Shesterkin
Formal analysis: Y. Tashiro, V. P. Shesterkin
Funding acquisition: D. Naito
Investigation: Y. Tashiro, M. Yoh, V. P. Shesterkin
Methodology: Y. Tashiro, T. Onishi
Project Administration: M. Yoh, V. P. Shesterkin, T. Shiraiwa, D. Naito
Software: T. Onishi
Supervision: M. Yoh, V. P. Shesterkin, T. Shiraiwa, T. Onishi
Validation: Y. Tashiro

© 2023. The Authors.

This is an open access article under the terms of the [Creative Commons Attribution License](#), which permits use, distribution and reproduction in any medium, provided the original work is properly cited.

Permafrost Wetlands Are Sources of Dissolved Iron and Dissolved Organic Carbon to the Amur-Mid Rivers in Summer

Y. Tashiro^{1,2} , M. Yoh³, V. P. Shesterkin⁴, T. Shiraiwa⁵, T. Onishi⁶, and D. Naito^{7,8}

¹United Graduate School of Agricultural Science, Tokyo University of Agriculture and Technology, Tokyo, Japan, ²Institute for Space–Earth Environmental Research, Nagoya University, Aichi, Japan, ³Institute of Agriculture, Tokyo University of Agriculture and Technology (Emeritus Professor), Tokyo, Japan, ⁴Institute of Water and Ecology Problems (FEB RAS), Khabarovsk Federal Research Center of the Far Eastern Branch of the Russian Academy of Sciences, Khabarovsk, Russia, ⁵Institute of Low Temperature Science, Hokkaido University, Hokkaido, Japan, ⁶Faculty of Applied Biological Sciences, Gifu University, Gifu, Japan, ⁷Center for International Forestry Research (CIFOR), Bogor, Indonesia, ⁸Faculty/Graduate School of Agriculture, Kyoto University, Kyoto, Japan

Abstract Dissolved iron (dFe) transported by the Amur River greatly contributes to phytoplankton growth in the Sea of Okhotsk. Nevertheless, there has been little research on the source of dFe to rivers, especially in the Amur-Mid Basin, which is situated in a sporadic permafrost area. In the Amur-Mid Basin, permafrost generally exists in wetlands in flat valleys, and these permafrost wetlands could be a source of dFe to rivers. To assess the importance of permafrost wetlands for dFe export, we conducted a local survey on land and soil characteristics of wetlands, and moreover analyzed the chemical composition (dFe, dissolved organic carbon [DOC], pH, and electrical conductivity [EC]) of 24 rivers with different watershed sizes in summer. As a result of local survey, the thickly accumulated peat soils in the permafrost wetland were almost saturated and rich in organic matter from the surface to a greater depth near the permafrost table. In addition, the coverage of such permafrost wetlands in watersheds showed significant positive correlations with dFe ($r^2 = 0.67$, $p = 1.7e-6$) and DOC ($r^2 = 0.48$, $p = 1.8e-4$) and a negative correlation with EC ($r^2 = 0.52$, $p = 7.7e-5$). The dFe concentration was also correlated well with DOC concentration ($r^2 = 0.68$, $p = 7.3e-7$) but not correlated with pH and watershed area. These findings are the first to indicate that permafrost wetlands in the Amur-Mid Basin considerably contribute to dFe and DOC export to rivers, and their coverage primarily determines riverine dFe and DOC concentrations in summer.

Plain Language Summary Dissolved iron (dFe) is a key factor that limits phytoplankton growth in the ocean. In the Amur-Okhotsk ecosystems, dFe transported by the Amur River greatly contributes to phytoplankton growth in the Sea of Okhotsk; however, there has been little research on the dFe source to rivers, especially in the Amur-Mid Basin, which is situated in a sporadic permafrost area. In this study, we focused on permafrost wetlands in the Amur-Mid Basin and investigated the soil characteristics and the relationship between wetland coverage and dFe concentrations in 24 watersheds. Permafrost wetlands contain waterlogged and organic-rich peat soils, and more importantly, their coverage clearly shows strong positive relationships with riverine dFe and dissolved organic carbon (DOC) concentrations. This is the first study to show that permafrost wetlands impact water chemistry in the Amur-Mid Basin, primarily as sources of dFe and DOC.

1. Introduction

Iron has a crucial role in a wide variety of phytoplankton metabolisms (Crichton, 2001; Sunda, 2012), and its availability can be a key factor for marine ecosystem. Martin and Fitzwater (1988) first revealed that iron deficiency is responsible for limiting phytoplankton growth despite the abundance of other nutrients in the north-east Pacific Oceans. Ensuing studies have also demonstrated that phytoplankton productivity in surface waters of high-nutrient low-chlorophyll (HNLC) regions is limited due to the extremely low concentration of dissolved iron (dFe) (Bruland & Lohan, 2003; Martin et al., 1989, 1990, 1994; Price et al., 1994; Takeda & Obata, 1995). In the past, dFe in sea-surface was believed to be supplied through the atmospheric iron dust deposition (Martin & Fitzwater, 1988). However, recent studies have indicated that dFe transport from rivers to coastal areas and the ocean is also important for phytoplankton primary production there (Laglera & Vandenberg, 2009; Matsunaga et al., 1998; Moore & Braucher, 2008; Nishioka et al., 2014), which suggested the need for understanding the source of dFe and the dFe transport processes to the oceans.

Visualization: Y. Tashiro

Writing – original draft: Y. Tashiro

Writing – review & editing: M. Yoh,
V. P. Shesterkin, T. Shiraiwa, T. Onishi,
D. Naito

To understand the biogeochemical cycle of Fe in terrestrial environments and land-river dFe transport, many studies have been conducted on the chemical species of dFe (Bergquist & Boyle, 2006; Ilina et al., 2013; Ingrid et al., 2006, 2018; Pokrovsky et al., 2005), seasonal variation in riverine dFe concentrations (Barker et al., 2014; Björkvald et al., 2008; Tashiro et al., 2020), and the source of dFe to rivers (Andersson & Nyberg, 2009; Björkvald et al., 2008; Matsunaga et al., 1998; Palviainen et al., 2015; Sarkkola et al., 2013). Most of the dFe in rivers are generally transported downstream in the form of iron complexes with organic matter, especially humic substances (Krachler & Krachler, 2021; Laglera & Vandenberg, 2009). Therefore, forests and wetlands with abundant organic matter play important roles in supplying rivers with dFe (Björkvald et al., 2008; Matsunaga et al., 1998; Palviainen et al., 2015). In boreal regions, wetlands (peatlands) often show a higher capacity to supply dFe to rivers than forests because a high groundwater level leads to the accumulation of humic substances due to suppressed decomposition of organic matter, which provides Fe-organic complexes under reducing conditions in the soil, as highlighted by previous studies focusing on land cover types of river catchments (Andersson & Nyberg, 2009; Björkvald et al., 2008; Palviainen et al., 2015; Sarkkola et al., 2013). For instance, Palviainen et al. (2015) studied dFe export from 27 catchments with different land cover types in Finland and found that the area of peatlands in the catchments was strongly related to high dFe export and that dFe export in peatland-dominated catchments was correlated with total organic carbon (TOC) export. This is in agreement with the study in permafrost terrains (Hirst et al., 2017) that investigated dFe and dissolved organic carbon (DOC) concentrations in the Lena River and tributaries, which drain a catchment almost entirely underlain by permafrost, and showed that riverine dFe and DOC concentrations were higher in the Central Plateau, where the peat bog soils are prevalent than those in other regions dominated by larch and salix forest. Olefeldt et al. (2014) also showed that riverine DOC concentration increased with increase in the coverage of lowlands, where peatlands are predominantly formed, in both permafrost and non-permafrost areas of western Canada. These findings highlight the importance of focusing on wetlands among various land cover types to identify the sources of dFe and DOC to rivers in permafrost areas.

The Sea of Okhotsk is a marginal sea of the northwest Pacific Ocean and is among the most biologically productive oceans worldwide (e.g., Sorokin & Sorokin, 1999). High biological productivity in the Sea of Okhotsk is considerably supported by the abundant dFe input through the Amur River (Nishioka et al., 2014; Shiraiwa, 2012; Suzuki et al., 2014). The Amur River Basin covers a huge area (approximately 2.1 million km²) in eastern Eurasia, including the eastern Mongolian Plateau, and forms the border between the Russian Far East and northeastern China. Although there are various types of natural environments in the Amur River Basin, previous studies have indicated some important dFe sources to rivers (Nagao et al., 2007; Wang et al., 2012). For example, the Sanjiang Plain, a large wetland in northeastern China, supplies abundant dFe to the Songhua and Ussuri rivers, which are large tributaries of the Amur River (Wang et al., 2012). It should be noted that intensive wetland reclamation to paddy field has been conducted in the Sanjiang Plain since the 1950s, and steady decline in riverine dFe concentration was observed from 1964 to 2008 (Pan et al., 2011). Wetlands in the Amur-Lower Basin from Khabarovsk to Nikolaevsk-na-Amure also greatly contribute to supplying dFe to the Amur River through tributaries (Nagao et al., 2007). Therefore, wide areas of the Amur-Lower Basin, including the Sanjiang Plain, are believed to be a particularly important dFe source for the Amur River. Some studies reported, however, that relatively high dFe concentrations were also observed in the Bureya River and the Zeya River, which drain the taiga zone in the Amur-Mid Basin (Nagao et al., 2007; Shamov et al., 2014) (Figure 1). More importantly, previous studies have shown that the Bureya and Zeya Rivers are rich in dFe and DOC, with a predominance of humic substances, especially the Bureya River; approximately 80% of dFe is complexed with DOC (Levshina, 2012). Nevertheless, the source of dFe to rivers in the Amur-Mid Basin remains poorly understood because of a lack of intensive research on land cover types and river water chemistry. A recent field research in the southern region of the Bureya River Basin found that wetlands are distributed in flat valleys, and more importantly permafrost is present underneath the wetlands (Tashiro et al., 2020). Furthermore, this study revealed that the dFe concentration in soil pore waters of the wetlands was more than 10 times higher than that in rivers throughout the season, indicating that permafrost wetlands in this region can be an important dFe source to rivers. To support this, we need to reveal the geographical and geological characteristics of wetlands in the Amur-Mid Basin and the relationship between permafrost wetland coverage and dFe concentration in watersheds. Given the ecological connectivity between the Amur River Basin and the Sea of Okhotsk through the land-river dFe transport, clarifying the source of dFe to rivers in the Amur-Mid Basin will lead to a better understanding and conservation of the Amur-Okhotsk ecosystem.

In this study, we conducted a local survey on the land and soil characteristics of wetlands, and moreover analyzed the chemical compositions (dFe, DOC, pH, and electrical conductivity (EC)) of 24 rivers in the southern region

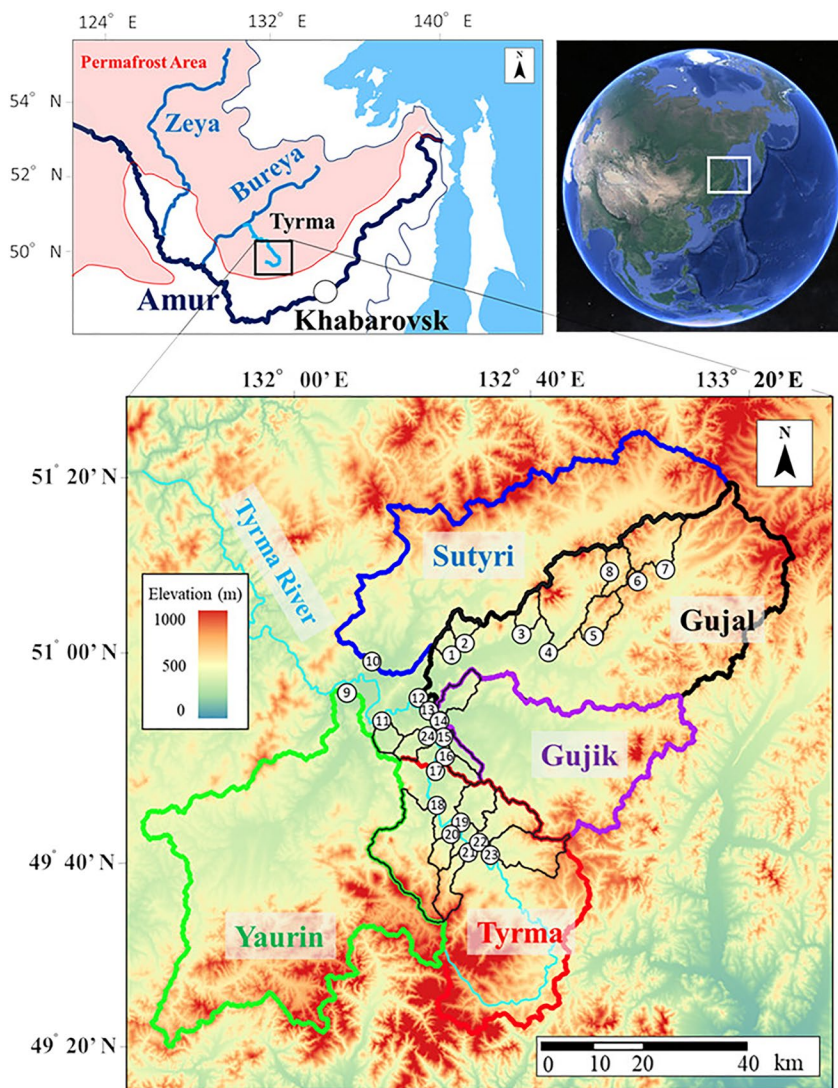


Figure 1. Location and elevation map of the Tyrma region. Permafrost area filled in light red was drawn in reference to Shamov et al. (2014). Areas enclosed by colored lines and numbers 1–24 show the catchment areas and the sampling sites of river waters. The elevation map was produced using Quantum Geographic Information System based on the ALOS World 3D-30 m data set provided by Japan Aerospace Exploration Agency.

of the Bureya River Basin. The main objective of this study was to develop knowledge on permafrost wetlands in the Amur-Mid Basin and determine their importance for dFe export by investigating the relationship between permafrost wetland coverage and riverine dFe concentration. To understand the land cover distribution of the study region we used remote sensing technique to create a reliable land cover map based on the local ground truth data. With this map we were able to calculate wetland coverage in river watersheds. This study is the first to provide detailed information on the land and soil characteristics of permafrost wetlands and land cover distribution on a regional scale in the Amur-Mid Basin, which are most likely the main drivers of river water chemistry in this region.

2. Materials and Methods

2.1. Site Description

The research was conducted in the Tyrma region, Verkhnebureinsky district of Khabarovsk territory (Figure 1). The mean annual air temperature is -1.96°C and annual precipitation is 654.6 mm. The Tyrma region is located



Figure 2. Typical vegetation type in the Tyrma region. (a) Wetland (*Mari*), (b) forest, (c) grassland. Detailed photos of the vegetation of the wetland (*Mari*) are shown in Figure S1 in Supporting Information S1.

just north of the permafrost boundary and in a sporadic permafrost area (Obu et al., 2019; Shamov et al., 2014). The Tyrma River is one of the main tributaries of the Bureya River, and the Tyrma region includes five large river watersheds, namely the Yaurin, Tyrma, Gujik, Gujal, and Sutyri Rivers (Figure 1).

Two types of vegetation are generally seen in different terrains in watersheds. Wetland is the main land cover type in the flat valleys, dominated by *Sphagnum* spp., ledum (*Ledum decumbens*), cowberry (*Vaccinium vitis-idaea* L.), bog blueberry (*Vaccinium uliginosum*), and scattered larches (*Larix gmelinii* var. *gmelinii*) (Figure 2a and Figure S1 in Supporting Information S1). White birches (*Betula platyphylla*) and Spruces (*Picea ajanensis*) forest covers widely the hillslopes (Figure 2b). Peat soils are generally formed at the topsoil layers in wetlands and forests, especially thick in wetlands owing to the accumulation of sphagnum mosses. Even more important is the fact that permafrost is found underneath a thick peat soil layer in wetlands (Tashiro et al., 2020). The wetland with these characteristics is called “*Mari*.” In this paper, the word “wetland” or “permafrost wetland” indicates *Mari*. In addition to forests and wetlands, grasslands are often found along large rivers (Figure 2c). Grasslands cover flat areas of land (floodplains) near large rivers and are characterized by herbaceous plants spreading over sediment deposits.

2.2. Transect Survey on Land and Soil Characteristics Across Wetland (*Mari*)

To investigate the land and soil characteristics of the wetland (*Mari*), we conducted a transect survey in the Sofron River watershed (River 1 in Figure 1) in September 2018. Because the Active Layer Thickness (ALT) reaches a maximum in September in this region, it is possible to determine whether permafrost exists below the ground surface. We established a 350 m transect of 17 points across the wetland in the valley to the forest on the upper hillslope to measure geographical features and confirm vegetation. At six of the 17 transect points (from N1 at the wetland edge on the riverside to N6 at the hillslope forest), we dug a pit and checked the vertical profile of soil temperature. Permafrost existence was determined by confirming the soil temperature of the permafrost table was 0°C using digital thermometer (FUSO, FUSO-372), and the depth from the ground surface to the permafrost table was defined as an ALT. The groundwater level was checked at these six points based on the depth at which water seeped out from the soil profile. In addition, soils at three different depths (surface, middle, and deep) of the soil profile were collected in polyethylene freezer bags to investigate the vertical profile of organic carbon content and moisture content. Soil samples were stored in a freezer until analysis.

2.3. Calculation of Normalized Difference Indices

A flowchart of the land cover classification process is shown in Figure 3. Landsat-8 data (Level2, Collection2, Tier1) with a spatial resolution of 30 m were used for land cover classification. Importing and processing of these data were conducted using the Google Earth Engine, which is a platform for scientific analysis and visualization of geospatial data sets (Gorelick et al., 2017). First, the Landsat-8 data from 2013 to 2021 were extracted. Then, data from the summer months (June, July, and August: JJA) were extracted. Finally, the medians of these JJA data were extracted to calculate the normalized difference indices, as described in the next paragraph.

To classify land cover using satellite image analysis, it is important to presume several surface conditions, such as vegetation, soil, and water. Thus, we calculated three indices using the JJA-median Landsat-8 data: normalized difference vegetation index (NDVI), normalized difference soil index (NDSI), and normalized difference water index (NDWI). The formulas used to calculate these three indices are as follows:

$$\text{NDVI} = (\text{Band5}_{\text{NIR}} - \text{Band4}_{\text{Red}}) / (\text{Band5}_{\text{NIR}} + \text{Band4}_{\text{Red}}) \quad (1)$$

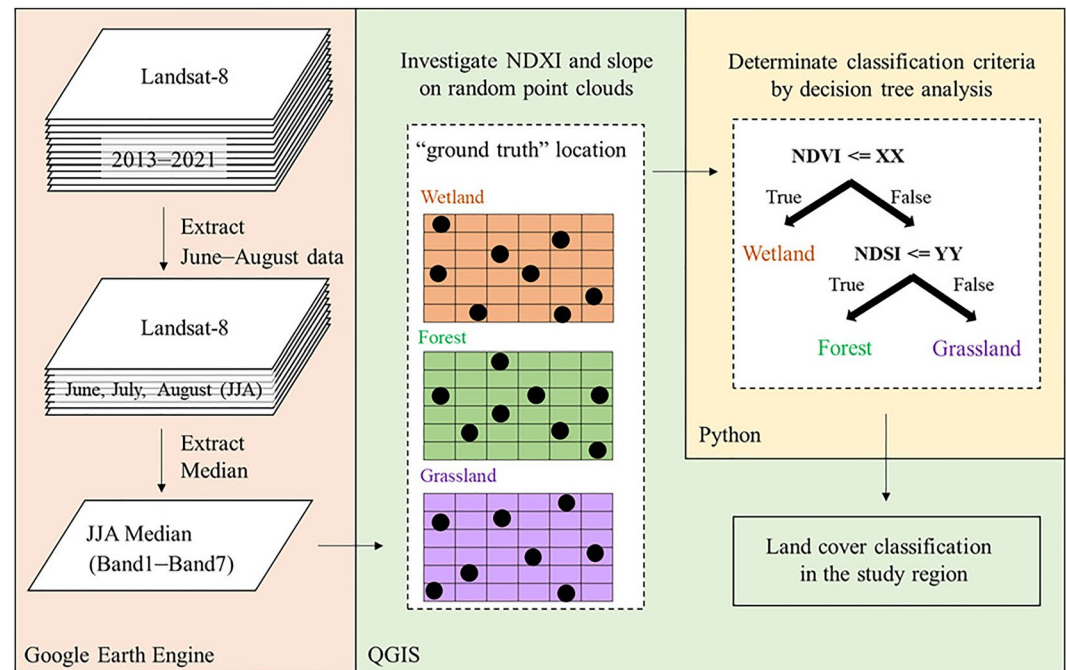


Figure 3. Schematic flowchart of several processes for landcover classification. The detailed explanations of the processes in Google Earth Engine, Quantum Geographic Information System, and Python are described in Sections 2.3, 2.4, and 2.5, respectively.

$$\text{NDSI} = (\text{Band6}_{\text{SWIR1}} - \text{Band5}_{\text{NIR}}) / (\text{Band6}_{\text{SWIR1}} + \text{Band5}_{\text{NIR}}) \quad (2)$$

$$\text{NDWI} = (\text{Band5}_{\text{NIR}} - \text{Band6}_{\text{SWIR1}}) / (\text{Band5}_{\text{NIR}} + \text{Band6}_{\text{SWIR1}}). \quad (3)$$

Each band of data is the JJA-median value. The band names and wavelengths of Landsat-8 are shown on the following website: <https://www.usgs.gov/faqs/what-are-band-designations-landsat-satellites>. NDVI, NDSI, and NDWI show different ranges depending on the vegetation activity, soil type, and water content of leaves (Gao, 1996; Takeuchi & Yasuoka, 2004; Tucker et al., 1985). In this study, the NDVI, NDSI, and NDWI were collectively described as NDXI. The code for extracting the JJA-median Landsat-8 data and calculating NDXI in Google Earth Engine is available in Figure S2 in Supporting Information S1.

2.4. Investigation of NDXI and Slope Across Different Vegetation Types

The investigation of NDXI in different vegetation types was conducted using the Geographic Information System (GIS) software Quantum GIS (QGIS version 3.20.0). In this study, we classified the land cover in the Tyrma region into three vegetation types: wetlands, forests, and grasslands (Figure 2). First, 30 random point clouds were generated in three areas that was dominated by these vegetations. Most importantly, the areas where random point clouds were generated were locations where we confirmed the actual vegetation type (ground truth) at the study site, including the wetland where the transect survey was conducted. A random point cloud is a tool to sample a certain amount of data in a given area, and we can specify the minimum distance between points (Figure S3 in Supporting Information S1). Here, we specified 30 m as the minimum distance to avoid generating points on the same grid of Landsat-8 data with a 30 m resolution. Random point clouds were generated in three ground truth areas for each vegetation type, that is, a total of 270 points (three vegetation types × three ground truth areas × 30 point clouds). Then, the NDXI values calculated using JJA-median Landsat-8 data were investigated for all 270 points. In addition to NDXI, the degree of slope at all 270 points was investigated. The slope data were created using ALOS World 3D-30 m data available free from the Japan Aerospace Exploration Agency (https://www.eorc.jaxa.jp/ALOS/jp/dataset/aw3d30/aw3d30_j.htm). The coordinates, NDXI values, and degree of slope for all 270 points are summarized in Table S1 in Supporting Information S1.

2.5. Determination of Classification Criteria by Decision Tree Algorithm

To classify land covers based on NDXI and slope, the criteria were determined by supervised machine learning. In this study, we utilized decision tree analysis in Python (version 3.8.5). A decision tree is an algorithm that classifies data gradually based on generated rules and outputs a tree-like graph. Of the data from all 270 points, 30% were used as test data, and the other 70% were used as learning data. Data classification was performed in three stages. The criteria obtained from the decision tree analysis were extrapolated to the entire Tyrma region, and land cover was classified into wetland (*Mari*), forest, and grassland. Then we checked whether the nine ground truth sites of wetlands (*Mari*) and permafrost existence, which were not included in the ground truth sites for NDXI calculation, were correctly classified as wetland (*Mari*) in the produced land cover map. The code for the decision tree analysis in Python is shown in Figure S4 in Supporting Information S1.

2.6. Sampling of River Waters

Water samples were collected from 24 rivers of different watershed sizes (4.7–3,253 km²) in July 2019 (Figure 1). Sampled waters were filtered using 0.45 μm cellulose acetate filters (ADVANTEC, DISMIC 25CS045AS) in the field and were stored in acid-washed propylene bottles for dFe analysis and other propylene bottles for DOC analysis. All water samples were refrigerated until analysis. In addition, pH and EC were measured using a portable pH meter (HORIBA, D-71S) and portable EC meter (HORIBA, ES-71), respectively, at the time of water sampling.

2.7. Chemical Analyses

The dFe concentration was determined using the 1,10-phenanthroline method (Russian International Technical Standards, 2006). First, 1 mL of 10% hydroxylammonium chloride was added to 50 mL of sample. Second, the mixture was boiled for 15–20 min until the volume reached 25 mL to separate the organic iron complexes into organic compounds and Fe (II). Third, after cooling, ammonium hydroxide was added until ~pH 4. Finally, 3 mL of ammonium acetate buffer and 1 mL of 1,10-phenanthroline were added, and ultrapure water was added until the volume reached 50 mL. Finally, 20 min after color development, the absorbance at 510 nm was measured using an ultraviolet–visible spectrophotometer (SHIMADZU UV mini-1240). In this study, we defined dFe as Fe, which was determined by this process. The detection limit for dFe by the 1,10-phenanthroline method was 0.02 mg L⁻¹. The DOC concentration was determined using a TOC analyzer (SHIMADZU TOC-LCSH) with detection limit of 0.1 mg L⁻¹. Potassium Hydrogen Phthalate (C₆H₄(COOK)(COOH)) (Nacalai Tesque) was used to prepare standard solutions for DOC measurement.

For the collected soil samples from wetland and forest, soil organic carbon content was determined using Tyurin's method (wet combustion) (Bel'chikova, 1975). The moisture content was calculated from the difference in mass before and after drying the soil at 103–105°C for at least 4 hr until the mass was constant.

2.8. Correlation Analysis Between the Coverage of Wetland and River Water Chemistry

Based on the produced land cover map (Sections 2.3–2.5), the coverage of wetlands (*Mari*) was investigated for each catchment area of the 24 sampled rivers. The correlation of water chemistry (dFe, DOC, and EC) and the coverage of wetlands (*Mari*) was assessed using linear regression analysis and non-linear regression analysis. In addition, the correlation between dFe and DOC concentrations and watershed area was investigated. For nonlinear regression analysis, three common functions (power, exponential, and logarithmic) were investigated to create an approximation curve. Both linear and nonlinear regression calculations were performed using the least-squares method with Microsoft Excel Solver (version 2021). The approximation line or curve with the highest coefficient of determination (r^2) was selected as the most suitable regression equation to represent the relationship between water chemistry and wetland coverage.

3. Results

3.1. Land and Soil Characteristics of Wetland (*Mari*) in Valley and Their Change Toward Forest on Hillslope

The results of the transect survey of wetlands (*Mari*), including geographical features, active-layer thickness, groundwater level, and predominant vegetation, are shown in Figure 4. The wetland entirely covers the valley

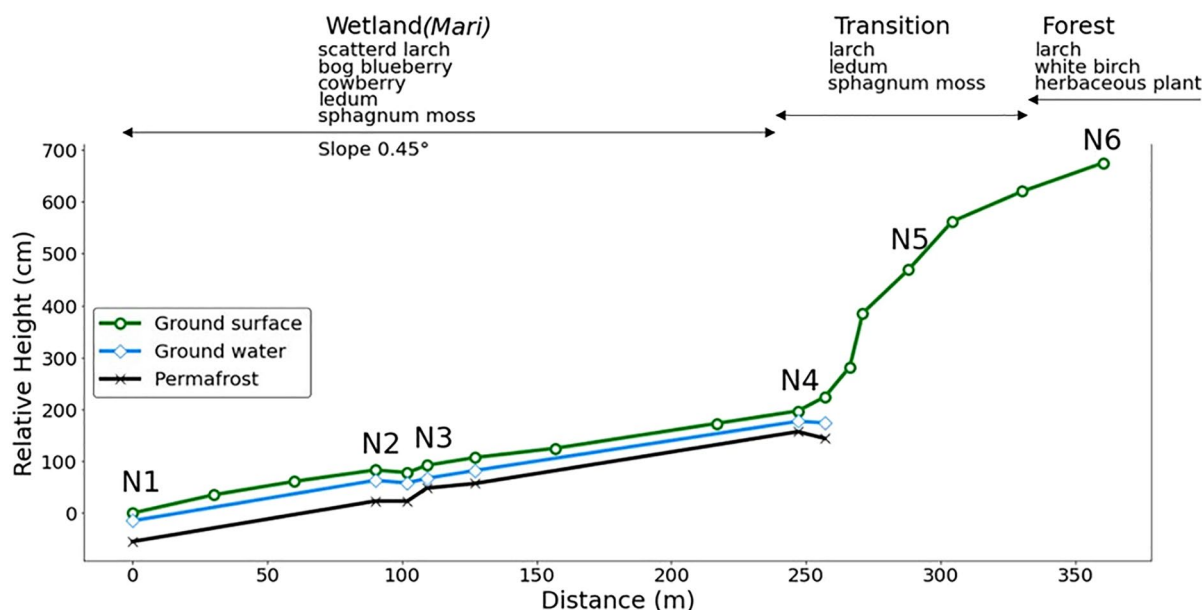


Figure 4. Vegetation, geographical features, groundwater level, and permafrost table across wetland (*Mari*) to the forest (September 2018). Point N1–N6 denotes the site where we dug a soil profile, checked a vertical profile of soil temperature (Figure S5 in Supporting Information S1), and examined organic carbon content and moisture weight content of soils at different depths (Table 1).

area from point N1 on the riverside to N4 at the foot of the hillslope, and the slope in the wetland zone was very flat (0.45°). Permafrost was generally confirmed at these four points in the wetland, as indicated by a decrease in soil temperature to 0°C at the depth of the permafrost table (Figure S5 in Supporting Information S1). The active-layer thickness was in the range of 40–60 cm. Peat soils thickly accumulated from the ground surface to the permafrost table, and the water seeped out from the peat profile near the surface (Figure S6a in Supporting Information S1). The organic carbon content in peat soils of the wetland ranged from 57 to 306 g C kg^{-1} (Table 1). In particular, the peat soils in the central part of the wetland (points N2 and N3) showed relatively high organic carbon content from the surface to the permafrost table. Groundwater was observed near the surface of the wetland and its level was in the range of 10–25 cm. In addition, the soil water content in peat soils of the wetland was almost 100% across the soil profile, except for the deeper soils at point N1, which was closest to the river.

An obvious vegetation change was confirmed toward the forest on the hillslope from the wetland. *Ledum* and *sphagnum* declined toward the forest; instead, herbaceous plants dominated the ground surface with larches and white birches. At points N5 and N6 on the hillslope, no decrease in soil temperature to 0°C was observed (Figure S5 in Supporting Information S1), indicating that permafrost no longer exists underneath the hillslope forests. Moreover, the soil profile in the forest showed a clear change in the soil characteristics with depth. At point N6 in the hillslope forest, there was the 10–20 cm accumulation of peat soil near the surface and a dry yellowish-brown soil layer was observed below the peat layer (Figure S6b in Supporting Information S1). The organic carbon content and soil water content at 0–10 cm depth were respectively 211 gC kg^{-1} and 90.2%, but both values greatly decreased with depth; the former was 6 gC kg^{-1} and the latter was 9.5% at 60–70 cm depth (Table 1). In summary, valley wetlands have waterlogged peat soils with high organic carbon content from the surface to permafrost, while hillslope forests have thin peat soils and underlying dry mineral soil layer with low organic carbon content.

3.2. Landcover Classification and Calculated Coverages of Wetland, Forest, and Grassland in Watersheds

The ranges of NDXI and slope of the point clouds in wetlands (*Mari*), forests, and grasslands are shown in Figure 5. Here, we focus on the differences in NDXI and slope in wetlands compared to those in forests and grasslands. In the wetland, the NDVI was in the range of 0.50–0.75, NDSI was -0.32 to -0.14 , and NDWI was -0.65 to -0.47 . The NDVI and NDWI in the wetland largely overlapped with those of the forest, indicating that NDVI and NDWI were not useful in distinguishing between wetlands and forests. In contrast, the NDSI in the

Table 1
Landscape, Active Layer Thickness (ALT), Organic Carbon Content and Weight Moisture Content at Different Depths at Each Transect Point

Site	Coordinates	Landscape	ALT (cm)	Depth (cm)	Organic carbon content (gC kg ⁻¹)	Weight moisture content (%)
N1	N 50.09770 E 132.36354	Wetland	55	0–10	228	90.1
				20–30	63	64.6
				50–60	57	65.0
N2	N 50.09778 E 132.36217	Wetland	60	0–10	306	100
				20–30	267	100
				50–60	297	99.2
N3	N 50.09790 E 132.36176	Wetland	50	0–10	291	103
				20–30	255	102
				40–50	252	100
N4	N 50.09802 E 132.36050	Wetland	40	0–10	251	102
				20–30	234	99.0
				30–40	177	99.3
N5	N 50.09798 E 132.35977	Wetland–	Not Detected	0–10	243	99.3
		Forest		30–40	14	33.7
				60–70	38	33.6
N6	N 50.09793 E 132.35875	Forest	Not Detected	0–10	210	90.2
				30–40	11	18.6
				50–60	6	9.5

wetland was clearly higher than that in forests and grasslands. The range of slope in the wetland was quite low at 0.43–4.31°. Compared with this, the forest clearly showed a higher range, but the grassland showed almost the same range as the wetland; accordingly, wetlands cannot be distinguished from grasslands by the slope alone. From these findings, the NDSI can be the most effective index for identifying the distribution of wetlands (*Mari*).

A graph of the decision-tree analysis is shown in Figure 6. The accuracy of this model for the test data was 92.6% (Figure S4 in Supporting Information S1). The accuracy rate is generally used to evaluate the prediction precision for unknown data and is calculated by dividing the number of correct classifications for the test data by the total number of test data (30% of 270 samples: 81). As shown in Figure 6, the NDSI was selected as a criterion in the first stage of the decision tree analysis. Based on $NDSI \leq -0.31$, most samples of the forest and grassland were classified in the true direction, whereas almost all samples of the wetland (*Mari*) were classified as false. This result indicates that wetlands can be distinguished from forests and grasslands, but only by NDSI. On the other hand, many forest and grassland samples remained in the box of true direction after the first stage. $NDWI \leq -0.674$ was used as a criterion to distinguish forest and grassland; most samples of grassland were classified in the true direction, while most samples of forest were classified as false. Finally, in the third stage, a small number of samples were classified according to slope, NDSI, and NDVI. From these results, it follows that the three-stage classification by the decision tree analysis based on NDSI and slope was sufficient to distinguish land cover as wetland (*Mari*), forest, and grassland.

The decision tree classification model was extrapolated for the Tyrma region, and the resulting land cover map is shown in Figure 7. Comparing this map with the elevation map (Figure 1), we can see that the wetland (*Mari*) widely covers valley areas. Grasslands also cover some of the valley areas, while forests mostly cover hillslopes from the valley edge to the ridge. More importantly, the nine ground truth sites of wetlands (*Mari*) and permafrost existence were all identified as wetland (*Mari*) in the land cover map (Figure S8 in Supporting Information S1). Note that these ground truth sites were not included in the process of producing the land cover map. Using this land cover map, the coverage percentages of wetlands (*Mari*), forests, and grasslands in the sampled river watersheds were calculated (Table 2). The calculated coverage of the wetland was 2.2%–59.4%, with the highest

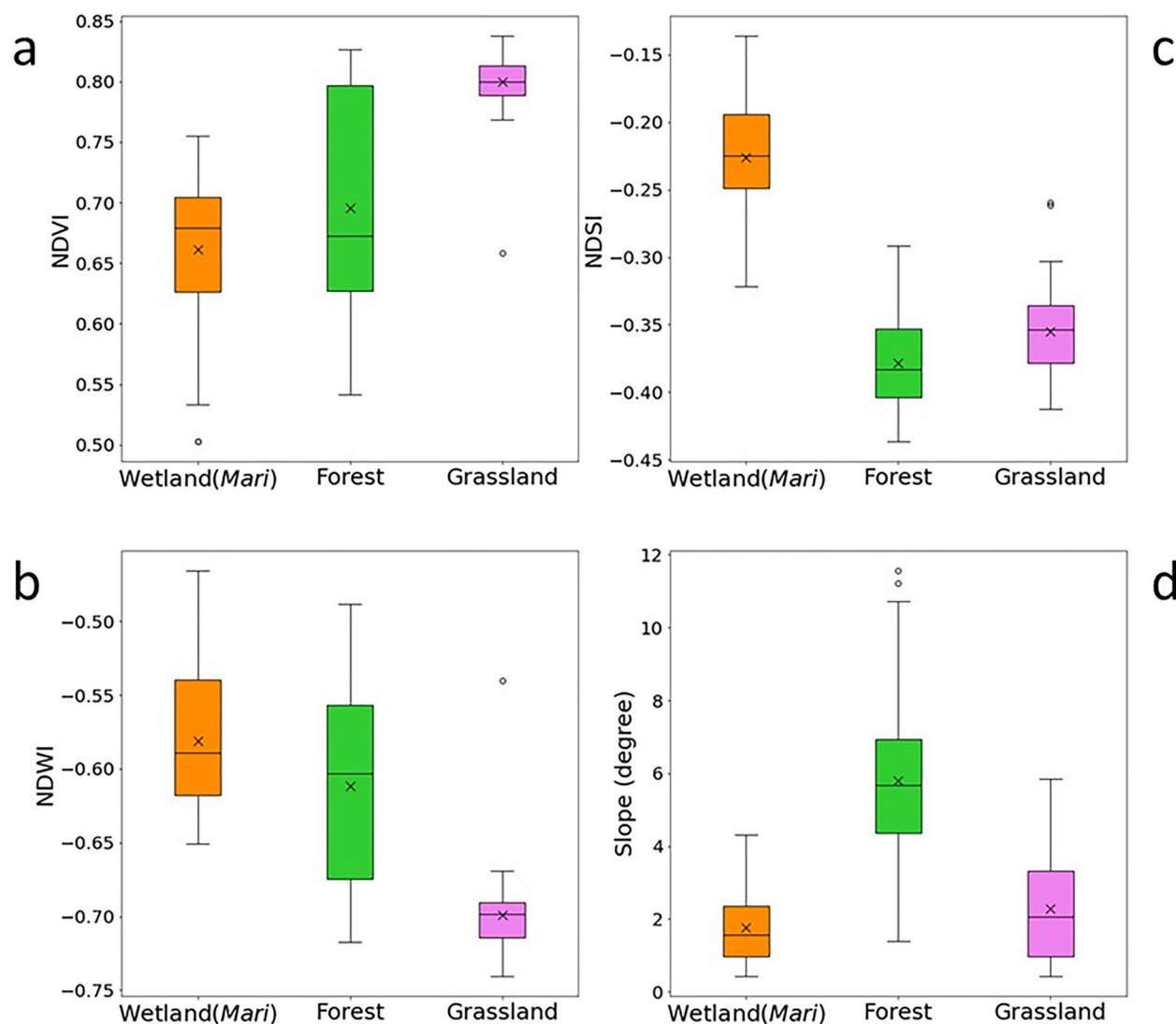


Figure 5. Box plot showing the comparison of (a) NDVI, (b) normalized difference soil index, (c) normalized difference water index, and (d) slope between wetland (*Mari*), forest, and grassland. The lower end of the box denotes the 25th percentile, the center line denotes the 50th percentile (exclusive median), and the upper end denotes the 75th percentile. The cross mark in the box denotes the average. Bar denotes the largest and smallest values within 1.5 times the interquartile range. Small dots outside boxes denote >1.5 times the interquartile range. $n = 90$ for each box plot. The underlying data for this figure are available in Table S1 in Supporting Information S1.

in the Kuvitikan River (number 15 in Table 2) and the lowest in the Kevity-Makit River (number 6). Looking at the location of watersheds, wetland coverage is especially higher in rivers 11–24 of the Tyrma River system (range 6.9–59.4, average 24.3) than in rivers 1–8 of the Gujal River system (range 2.2–17.3, average 8.0). In all watersheds except the Kuvitikan River (number 15), the forest was the most dominant landcover (20.6%–96.7%). The range of grassland coverage was 1.1%–31.9%, which was relatively smaller than that of the wetland.

3.3. River Water Chemistry and Their Relationship With the Coverage Percentage of Wetlands (*Mari*) in the Watersheds

Twenty-four sampled rivers with different watershed sizes in the Tyrma region showed a variety of water chemistries (Table 2) with wide concentration ranges for dFe ($0.02\text{--}0.54\text{ mg L}^{-1}$) and DOC ($7.4\text{--}29.5\text{ mg L}^{-1}$). The EC was also in a wide range of $2.89\text{--}14.00\text{ mS m}^{-1}$. The pH varied in the near-neutral range of 6.61–8.01. We found that the coverage percentage of wetlands (*Mari*) was significantly correlated with dFe, DOC, and EC (Figure 8). The riverine dFe concentration showed a significant increase with increasing wetland coverage ($r^2 = 0.67$,

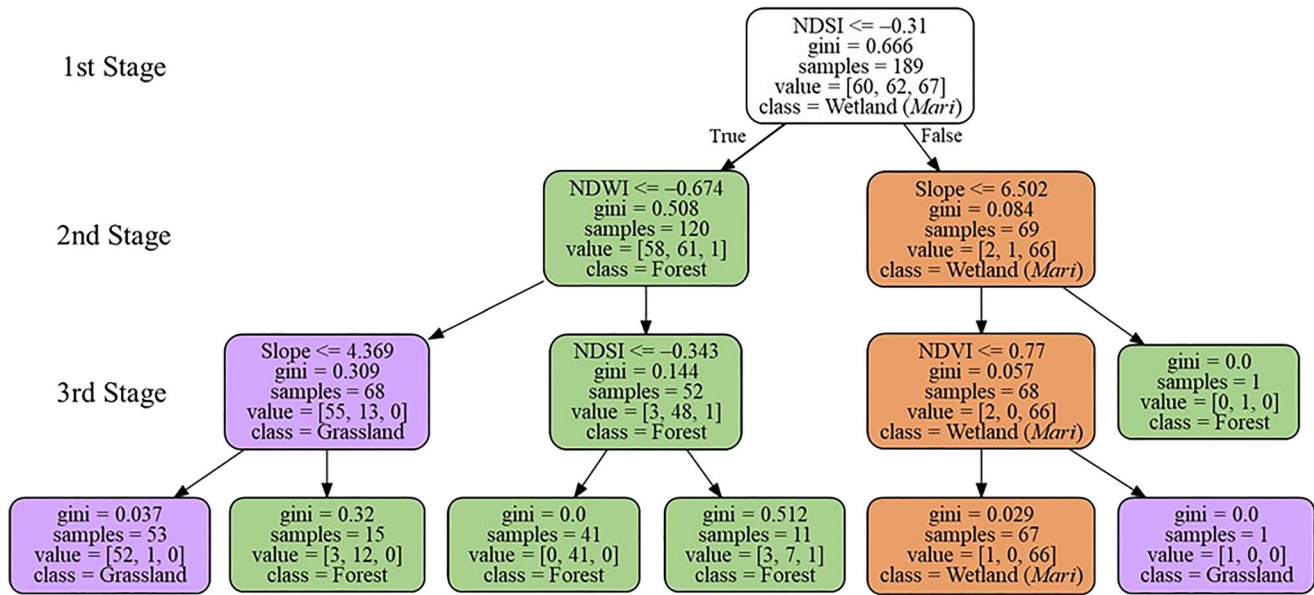


Figure 6. Output graph of the decision tree analysis. The contents in each box are: the top part is the classification criterion; gini denotes the Gini coefficient; samples denote the total number of samples for classification—189 in the box at the first stage means 70% of the total samples (270), which is used as learning data; value denotes the number of samples, from left to right, Grassland, Forest, and Wetland (*Mari*); class denotes the greatest share of classified samples. The box colors: orange, green, and purple represent the class: wetland, forest, and grassland, respectively.

$p = 1.7e-6$). The DOC concentration also correlated well with wetland coverage ($r^2 = 0.48$, $p = 1.8e-4$). In contrast, riverine EC significantly decreased with increasing wetland coverage ($r^2 = 0.52$, $p = 7.7e-5$). We also found that riverine dFe concentration had a significant positive correlation with DOC concentration ($r^2 = 0.68$, $p = 7.3e-7$) and a significant negative correlation with EC ($r^2 = 0.65$, $p = 2.1e-6$), but no correlation with pH ($r^2 = 1.3e-4$, $p = 0.96$). There was no correlation between the watershed area and dFe and DOC concentrations (dFe $r^2 = 0.008$, $p = 0.67$; DOC $r^2 = 0.002$, $p = 0.84$) (Figure S7 in Supporting Information S1).

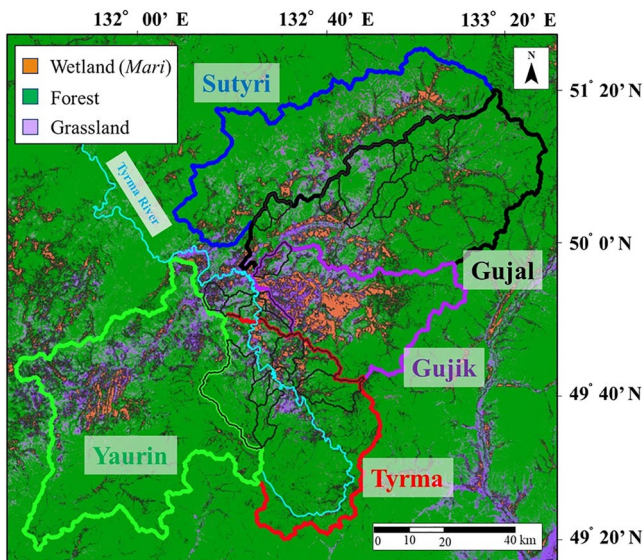


Figure 7. Landcover map in the Tyrma region as a result of extrapolating the decision-tree's classification model. Orange areas denote the places classified into wetland (*Mari*). Similarly, green areas denote forest, and purple areas denote grassland. Areas enclosed by color and black lines show the catchment areas of the sampled rivers.

4. Discussion

4.1. Permafrost Regime in the Tyrma Region and Comparison of dFe and DOC Concentrations in Other Similar Permafrost-Regime Regions

Our transect survey displayed the continuous distribution of permafrost in the wetland and its disappearance toward the forest on hillslopes with changes in vegetation and soil characteristics. General existence of permafrost underneath the wetland (*Mari*) is likely due to the reduction in heat transfer between atmosphere and soil by sphagnum mosses. According to Fisher et al. (2016) that investigated the influence of vegetation and land characteristics (slope, elevation, leaf area index of trees and shrubs, organic soil layer thickness, and moss layer thickness) on ALT, the tree leaf area index and moss layer thickness predominantly limit the ALT by reducing the downward heat flux. Given that larches are scattered in the wetland (*Mari*) in the Tyrma region, sphagnum mosses are expected to suppress the soil temperature rise rather than larch leaves. Lower soil temperatures were observed in wetland soils than in forest soils throughout the warm season in the Tyrma region (Tashiro et al., 2020).

Considering the land cover map produced in this study (Figure 7) was based on NDSI and slope in the ground truth areas, the areas determined to be wetlands likely have similar vegetation and soil characteristics as wetlands (*Mari*) seen in the transect survey. On the basis of permafrost existence

Table 2
List of Sampled Rivers, Watershed Area, Coverage of Landcovers, and Water Chemistry

Number	Date	River	Watershed (km ²)	Wetland (%)	Forest (%)	Grassland (%)	pH	dFe (mg L ⁻¹)	DOC (mg L ⁻¹)	EC (mS m ⁻¹)
1	24 July	Sofron	23.3	5.6	89.1	5.8	7.33	0.160	17.3	3.82
2	24 July	Yakagulin	34.0	5.8	82.8	11.6	7.18	0.183	16.3	4.29
3	24 July	No Name	43.9	17.3	64.6	18.8	7.23	0.139	16.0	4.17
4	24 July	Kevity	323.0	7.2	79.2	14.0	6.74	0.081	11.2	7.14
5	24 July	Jangsovo	69.8	6.5	90.5	3.1	6.88	0.071	12.5	9.82
6	24 July	Kevity-makit	4.7	2.2	96.7	1.1	7.33	<0.02	9.1	14.00
7	25 July	Sula	140.9	11.7	84.7	4.0	7.50	0.068	12.2	5.18
8	25 July	Kevity (upstream)	56.1	7.8	88.9	4.0	7.36	0.120	12.6	7.91
9	26 July	Yaurin	3,253	16.5	71.7	9.9	7.13	0.380	19.0	3.90
10	26 July	Sutyri	2,129	14.7	76.3	9.3	6.96	0.185	13.4	4.17
11	27 July	No Name	42.1	40.2	28.7	31.9	7.51	0.330	24.4	3.90
12	27 July	Gujal	2,689	15.8	76.2	8.3	7.37	0.123	15.2	5.30
13	27 July	Allan	55.7	31.8	40.1	28.7	6.69	0.500	29.5	2.89
14	27 July	Gujik	1,383	34.8	54.0	11.4	6.84	0.360	18.4	3.42
15	27 July	Kuvitikan	32.4	59.4	20.6	20.5	7.46	0.540	21.0	3.09
16	27 July	Kuvitikan Verkhny	34.8	25.4	56.0	18.8	7.11	0.280	18.7	4.32
17	26 July	Tyrma	2,072	16.5	76.9	6.9	7.47	0.145	14.9	5.63
18	27 July	Kovun	279.6	10.3	82.5	7.7	7.23	0.072	12.0	5.97
19	27 July	Right Talanja	79.4	41.8	44.0	14.6	7.83	0.360	19.7	4.13
20	27 July	Talanja	38.4	7.0	78.0	15.2	7.55	0.280	13.9	6.78
21	28 July	Tokchka-birakan	65.4	6.9	86.6	6.6	7.55	0.053	7.4	6.60
22	28 July	Small Nigba	98.5	29.8	63.2	7.4	7.59	0.360	16.9	6.21
23	28 July	Big Nigba	140.4	22.2	76.0	2.1	8.01	0.093	10.0	9.02
24	29 July	Talkanji	42.1	7.2	64.1	29.3	6.61	0.046	12.9	8.82

underneath the wetland (*Mari*) in this study and the previous study (Tashiro et al., 2020), wetlands can be a proxy for permafrost distribution in the Tyrma region. This is supported by agreement between landcover map and our ground truth in several sites (Figure S8 in Supporting Information S1), although more ground truth is needed to ensure the distribution agreement between wetlands (*Mari*) and permafrost. Given this perspective, the permafrost coverage percentage in the Tyrma region can be estimated at around 15%–35% from the calculated wetland coverage in the large river watersheds (the Yaurin, Gujik, Gujal, Sutyri, and Tyrma Rivers) (Table 2). This coverage corresponds to the permafrost regime (sporadic permafrost distribution: 10%–50%) estimated by Obu et al. (2019) using a hemispheric-scale model.

There have been some studies on river water chemistry in sporadic permafrost areas, for example, in the Ob River flowing north and west across the western Siberian lowlands. Pokrovsky et al. (2016) showed that riverine dFe concentrations in sporadic permafrost regions (around N60°–N62°) in summer were in the range of 0.5–3.5 mg L⁻¹, and Vorobyev et al. (2017) showed that they were 0.2–1.8 mg L⁻¹, respectively (filter size was 0.45 μm as in this study). Compared with these data in the Ob River Basin, riverine dFe concentrations in the Tyrma regions were relatively low (<0.02–0.540 mg L⁻¹). However, riverine DOC concentrations in the Tyrma region and those in sporadic permafrost regions in the Ob River Basin are almost in the same range in summer: 7.4–29.5 mg L⁻¹ in the Tyrma region and 6–33 mg L⁻¹ in the Ob region (Pokrovsky et al., 2015; Vorobyev et al., 2017) (filter size was 0.45 μm). One of the reasons for the difference in dFe concentration between the Tyrma and Ob regions, despite the same permafrost regime, might be the soil profile in the active layer. Because soil thawing in summer allows water to interact with the mineral soil horizon under the peat soil layer, this can increase dFe discharge into rivers, as is known in Siberian watersheds with sporadic or less permafrost distribution (Bagard et al., 2011; Pokrovsky et al., 2016; Vorobyev et al., 2017). In the Tyrma region, thick peat soil layers

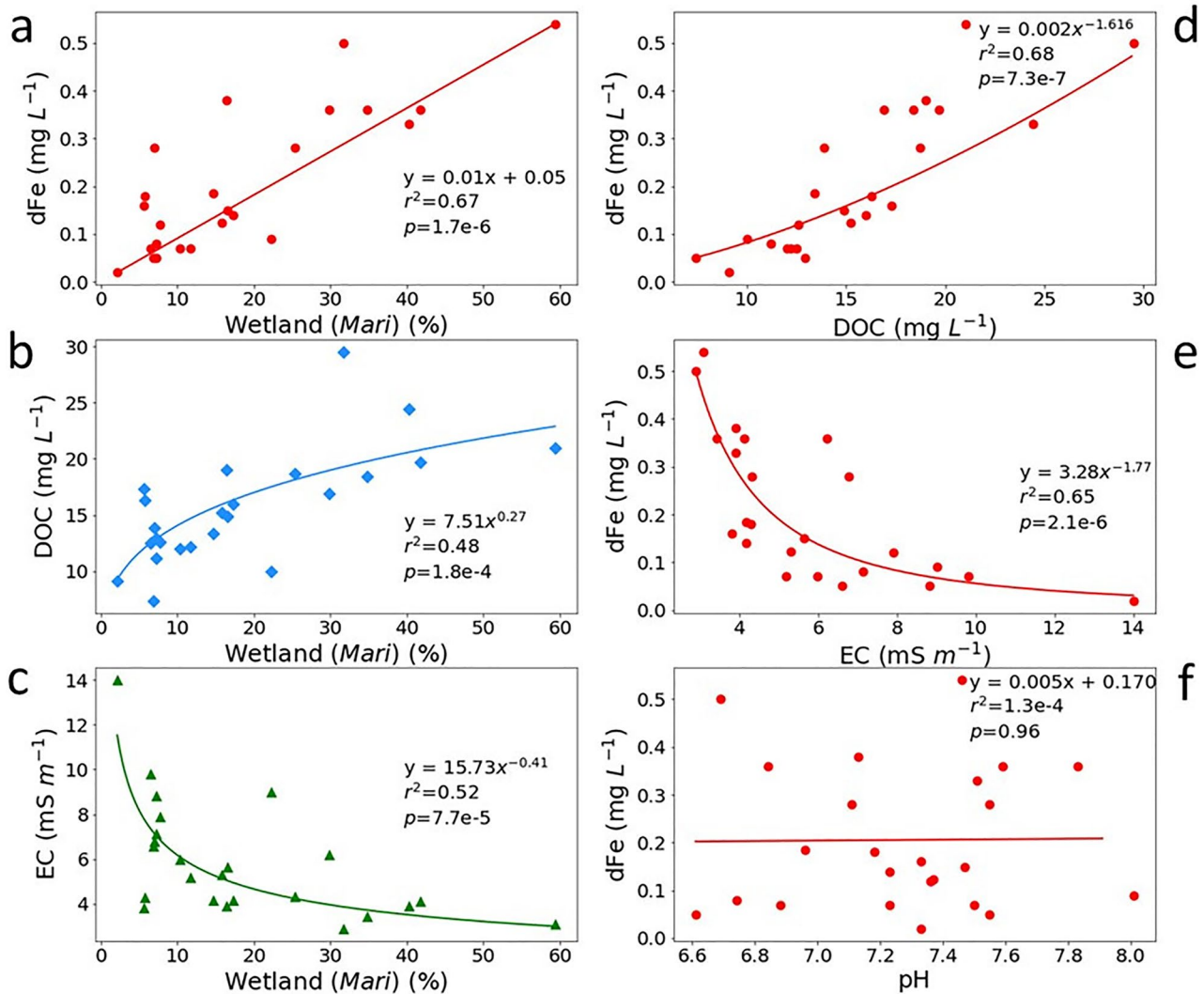


Figure 8. Variations in (a) dFe concentration, (b) dissolved organic carbon (DOC) concentration, and (c) electrical conductivity (EC) with an increase in the coverage of wetland (*Mari*). Figure panels on the right-hand side show variations in dFe concentration with increases in (d) DOC concentration, (e) EC, and (f) pH.

from the surface to near the permafrost table are formed in the wetland (Tashiro et al., 2020); therefore, water interaction with mineral soils may be restricted in the flow path from the wetlands (*Mari*) to the rivers in summer.

4.2. Role of Permafrost Wetland (*Mari*) in Supplying dFe and DOC to Rivers

The transect survey revealed that soil characteristics of the wetland (*Mari*) in valley and the forest on hillslope were quite different; the peat soils of the wetland were waterlogged and rich in organic carbon, whereas mineral soils of the forest were dry and poor in organic carbon (Figure 4 and Table 1). Such soil characteristics in the wetland (*Mari*) in the Tyrma region, similar to other boreal sphagnum peatlands, are favorable for dFe (Fe-organic complex) production under reducing conditions (Björkvald et al., 2008; Krachler et al., 2016; Krachler & Krachler, 2021). In fact, considerably higher dFe concentration was observed in the soil pore waters of the wetlands (*Mari*) compared to rivers in summer (Tashiro et al., 2020). Moreover, our fine-scale land cover map enabled us to calculate the percentages of land cover and detect a relationship between wetland coverage and water chemistry. Most of the sampled river watersheds were mainly covered with forest, and the wetland coverage was relatively smaller than that of the forest; nevertheless, wetland coverage had a large influence on dFe and DOC concentrations and EC in rivers in the Tyrma region (Figure 8). Since EC is an index showing the amount of dissolved ions present in the water, these results suggest that dFe- and DOC-rich and mineral-poor water are

supplied from peat soils of wetlands (*Mari*) in valley, and wetland coverage in watersheds primarily determines dFe and DOC concentrations in summer. The fact that wetlands (*Mari*) widely cover flat valleys with strong hydrological connectivity to rivers may be another reason for the strong correlation between wetland coverage and water chemistry. Our findings agree well with those of previous studies that have focused on the water chemistry of forest- and wetland (peatland)-dominated watersheds in other boreal regions (Björkvald et al., 2008; Palviainen et al., 2015; Sarkkola et al., 2013). Similar findings were also reported in northwestern Canada, where peat bogs are generally underlain by permafrost (Olefeldt et al., 2013, 2014).

We also found a significant positive correlation between riverine dFe and DOC concentrations (Figure 8d), indicating that wetland(*Mari*)-derived dFe mainly comprises Fe-organic complexes that are stable in river waters with neutral pH and can be transported to the ocean (Krachler & Krachler, 2021; Tipping, 2002). This is consistent with Levshina (2012), who found the high ratio of Fe-organic complexes to total dFe in the Zeya and Bureya Rivers in summer. The importance of Fe-organic complexes in the Tyrma region is also supported by the range of pH values (6.61–8.01) in the sampled rivers (Figure 8f and Table 2). Compiled plots of Fe loading and pH from boreal freshwater samples showed that Fe loading for pH < 6 increased with decreasing pH, but Fe loading for neutral pH from 6 to 8 exhibited a wide variation due to the presence of Fe-organic complexes in boreal freshwater, which are sufficiently stable to suppress the precipitation of iron (oxy)hydroxides (Neubauer et al., 2013).

There was no effect of watershed area on riverine dFe and DOC concentrations in the summer (Figure S7 in Supporting Information S1). A previous study that observed seasonal variations in dFe and DOC concentrations in rivers in the Tyrma region also showed that dFe/DOC molar ratio was similar between a small river and large rivers from May to August (Tashiro et al., 2020). However, they also found that dFe/DOC molar ratio in the large rivers maintained higher values than that in the small river in autumn (September and October). Our results and these findings suggest that wetlands (*Mari*) act as source of dFe (mainly Fe-organic complexes) to rivers in summer, whereas another source of dFe apart from DOC mobilization exists in large watersheds in autumn. Given that large rivers are expected to be more influenced by groundwater feeding (Bagard et al., 2011), increased Fe(II)-rich groundwater input through taliks may be another source of dFe in autumn. In the Tyrma region, the ALT reaches its maximum in September, and the river discharge decreases because of less rainfall in this month (Tashiro et al., 2020). Therefore, the effect of watershed area on riverine dFe concentration is expected to be greater in autumn and winter, when river water is predominantly fed by deep groundwater. Previous studies have provided a context on this process; Fe(II) input through groundwater produces organically bound Fe(III) colloids when mixed with organic matter-rich river water in the hyporheic zone (Ilina et al., 2013; Pokrovsky et al., 2016). In the western Siberian watersheds, no correlation between watershed area and dFe and DOC concentrations in summer was also reported (Pokrovsky et al., 2015, 2016), which is in agreement with our results. In contrast, a clear decrease in DOC export with watershed area was found in Scandinavian rivers (Ågren et al., 2007). Although many factors may cause this contrast between permafrost regions and Scandinavia, one of the reasons for this could be the low biodegradability of DOC in permafrost-affected rivers. Pokrovsky et al. (2015) found that the stable carbon isotope composition of dissolved inorganic carbon ($\delta^{13}\text{C-DIC}$), a proxy for the breakdown of organic matter by microorganisms, was independent of the watershed area and water residence time in Western Siberia. The low biodegradability of DOC in permafrost-affected rivers is often represented as abundant lignin-derived phenol, as highlighted for studies in the Yenisey River Basin and the Yukon River Basin (Kawahigashi et al., 2004; Spencer et al., 2008). Moreover, aromatic DOC including phenolic compounds is more leached from wetlands soils compared to forest soils (Ågren et al., 2008; Kalbitz et al., 2003). These drivers related to dFe and DOC dynamics behind the importance of permafrost wetlands (*Mari*) are outside the focus of this study but deserve further research to better understand the role of permafrost wetlands as sources of dFe and DOC to rivers.

4.3. Importance of Permafrost Wetland (*Mari*) in the Amur-Mid Basin as Source of dFe to the Amur River

Overall, the results of this study indicate that permafrost wetlands (*Mari*) in the Amur-Mid Basin are important sources of dFe and DOC to rivers in summer. According to monitoring of dFe concentration at several stations along the main stem of the Amur River, dFe flux from the Amur-Mid Basin to Lower Basin in summer was estimated to be $2.86 \times 10^8 \text{ g day}^{-1}$, which dominates approximately 33% of dFe flux at the station closest to the river mouth (Nagao et al., 2007). Additionally, Levshina (2012) found that the share of Fe-organic

complexes to total dFe concentration in the Bureya River, which is a major tributary in the Amur-Mid Basin, was higher than those in tributaries in the Amur-Lower Basin. This indicates that dFe, transported from the Amur-Mid Basin, is highly stable during the river transport. In recent years, it is generally believed that non-permafrost wetlands in the Amur-Lower Basin are source of dFe to the Amur River (Nagao et al., 2007; Pan et al., 2011; Wang et al., 2012). To this understanding, this study proposes for the first time that permafrost wetlands (*Mari*) in the Amur-Mid Basin are also important source of dFe to the Amur River and perhaps to the Sea of Okhotsk.

The strong relationship between the coverage of permafrost wetlands (*Mari*) and water chemistry (Figure 8) supports the possibility that permafrost degradation influences riverine dFe concentration due to the alternation of hydrological processes and iron dynamics (Shamov et al., 2014). This is beyond the scope of this study, but it may be worth mentioning the future change in dFe discharge from permafrost wetlands to rivers. In general, permafrost prevents the downward infiltration of water and consequently constrains the path of water to the surface of the active layer (Olefeldt et al., 2014; Petrone et al., 2006; Pokrovsky et al., 2015, 2016). Considering this fact, a possible scenario is that deeper flow paths due to permafrost degradation result in enhanced interactions of water with a deep mineral soil layer, which contains higher amounts of dFe and aquatic Fe(II) than the peat soil layer (Herndon et al., 2015; Jessen et al., 2014), and increased dFe discharge to rivers. Although the mineral soil layer was not universally confirmed in the wetland (*Mari*) in this study, permafrost thawing likely accelerates the mobilization of deeply frozen iron minerals. This is contrast scenario to non-permafrost wetlands; lower water table and less reducing conditions in wetland soils under a warming climate are expected to decrease dFe discharge to rivers (Dillon & Molot, 2005; Landre et al., 2009). At present, it is difficult to accurately predict the future change in riverine dFe concentration in the Amur-Mid Basin because of a lack of knowledge of iron dynamics and permafrost geochemistry. Nevertheless, this study emphasizes the need for further research about the influence of permafrost degradation on dFe concentration in the Amur-Mid rivers because wetland-derived dFe greatly contributes to the marine ecosystem in the Sea of Okhotsk (Nishioka et al., 2014; Shiraiwa, 2012; Suzuki et al., 2014).

5. Conclusions

To assess the importance of permafrost wetlands, called *Mari*, as a dFe source to rivers in the Tyrma region, we conducted a local transect survey on the land and soil characteristics from wetland to forest. Permafrost existence was generally confirmed under the surveyed wetland, and the thickly accumulated peat soils of the wetland are almost saturated and rich in organic carbon. Moreover, our combined approach of field surveys and remote sensing technique allowed us to detect the relationship between coverage of permafrost wetland (*Mari*) and river water chemistry: dFe and DOC concentrations significantly increased, but EC decreased with an increase in wetland coverage in the watershed. The dFe concentration was also significantly correlated with DOC concentration, but not with pH and watershed area. Based on these findings, we conclude that permafrost wetlands (*Mari*) in valley areas play an important role in supplying Fe-organic complexes to rivers, and their coverage primarily determines the dFe and DOC concentrations in summer. To the best of our knowledge, this study is the first to provide the land and soil characteristics of wetland and forest in the Amur-Mid Basin and show the relationship between the coverage of permafrost wetlands (*Mari*) and river water chemistry in this region. Given that permafrost degradation is predicted to occur due to ongoing climate change, further research is required to assess the influence of permafrost degradation on the watershed hydrological cycle, iron dynamics, and riverine dFe concentration in the Amur-Mid Basin, which may have the potential to change the amount of dFe discharged to the Sea of Okhotsk.

Data Availability Statement

All numeric data about land and soil characteristics in wetland and forest (Figure 4 and Table 1), water chemistry (Table 2), vertical profiles of soil temperature (Figure S5 in Supporting Information S1), and NDXI and slope data (Figure S7 in Supporting Information S1) are available at Figshare repository via (Tashiro et al., 2023) <https://doi.org/10.6084/m9.figshare.23735487.v1> with CC-BY 4.0.

Acknowledgments

We gratefully acknowledge T. Kubo for helping with the remote sensing technique and S. I. Levshina for soil analyses in the Institute of Water and Ecology Problems. We would like to thank D. N. Markina for study assistant as an interpreter. We are especially grateful to N. P. Mikhailov for supporting us throughout the field research in the Tyrra region. We are also grateful to three anonymous reviewers for their valuable comments which greatly improved this manuscript. This research was partially funded by the Center for International Forestry Research (CIFOR) project titled “Enhancing climate-resilient livelihoods in boreal and tropical high carbon forests and peatlands,” Japan Society for the Promotion of Science KAKENHI (Grant 19H05668) project titled “Pan-Arctic Water–Carbon Cycles (PAWCs)” (<https://enpawcs.home.blog/>), and Japan Society for the Promotion of Science KAKENHI (Grant 19H01976) project titled “Elucidation and prediction of spatiotemporal variations of PM2.5 due to wildfires over the Far Eastern region, and the assessment of PM2.5 impact on human activities.” We would like to thank Editage (www.editage.com) for English language editing.

References

- Ågren, A., Buffam, I., Berggren, M., Bishop, K., Jansson, M., & Laudon, H. (2008). Dissolved organic carbon characteristics in boreal streams in a forest-wetland gradient during the transition between winter and summer. *Journal of Geophysical Research*, *113*(3), 1–11. <https://doi.org/10.1029/2007JG000674>
- Ågren, A., Buffam, I., Jansson, M., & Laudon, H. (2007). Importance of seasonality and small streams for the landscape regulation of dissolved organic carbon export. *Journal of Geophysical Research*, *112*(3), 1–11. <https://doi.org/10.1029/2006JG000381>
- Andersson, J., & Nyberg, L. (2009). Using official map data on topography, wetlands and vegetation cover for prediction of stream water chemistry in boreal headwater catchments. *Hydrology and Earth System Sciences*, *13*(4), 537–549. <https://doi.org/10.5194/hess-13-537-2009>
- Bagard, M. L., Chabaux, F., Pokrovsky, O. S., Viers, J., Prokushkin, A. S., Stille, P., et al. (2011). Seasonal variability of element fluxes in two Central Siberian rivers draining high latitude permafrost dominated areas. *Geochimica et Cosmochimica Acta*, *75*(12), 3335–3357. <https://doi.org/10.1016/j.gca.2011.03.024>
- Barker, A. J., Douglas, T. A., Jacobson, A. D., McClelland, J. W., Ilgen, A. G., Khosh, M. S., et al. (2014). Late season mobilization of trace metals in two small Alaskan arctic watersheds as a proxy for landscape scale permafrost active layer dynamics. *Chemical Geology*, *381*, 180–193. <https://doi.org/10.1016/j.chemgeo.2014.05.012>
- Bel'chikova, N. P. (1975). Determination of humus in soil by I.V. Tyurin method. In A. V. Sokolov (Ed.), *Agrochemical methods of soil studies* (pp. 56–62). Nauka. (In Russian).
- Bergquist, B. A., & Boyle, E. A. (2006). Iron isotopes in the Amazon River system: Weathering and transport signatures. *Earth and Planetary Science Letters*, *248*(1–2), 54–68. <https://doi.org/10.1016/j.epsl.2006.05.004>
- Björkvald, L., Buffam, I., Laudon, H., & Mörth, C. M. (2008). Hydrogeochemistry of Fe and Mn in small boreal streams: The role of seasonality, landscape type and scale. *Geochimica et Cosmochimica Acta*, *72*(12), 2789–2804. <https://doi.org/10.1016/j.gca.2008.03.024>
- Bruland, K. W., & Lohan, M. C. (2003). 6.02 – Controls of trace metals in seawater. *Treatise on Geochemistry*, *6*, 23–47. <https://doi.org/10.1016/B0-08-043751-6/06105-3>
- Crichton, R. (Ed.). (2001). *Inorganic biogeochemistry of iron metabolism: From molecular mechanisms to clinical consequences*. John Wiley.
- Dillon, P. J., & Molot, L. A. (2005). Long-term trends in catchment export and lake retention of dissolved organic carbon, dissolved organic nitrogen, total iron, and total phosphorus: The Dorset, Ontario, study, 1978–1998. *Journal of Geophysical Research*, *110*(G1), G01002. <https://doi.org/10.1029/2004jg000003>
- Fisher, J. P., Estop-Aragonés, C., Thierry, A., Charman, D. J., Wolfe, S. A., Hartley, I. P., et al. (2016). The influence of vegetation and soil characteristics on active-layer thickness of permafrost soils in boreal forest. *Global Change Biology*, *22*(9), 3127–3140. <https://doi.org/10.1111/gcb.13248>
- Gao, B. (1996). NDWI A normalized difference water index for remote sensing of vegetation liquid water from space. *Remote Sensing of Environment*, *58*(3), 257–266. <https://doi.org/10.24059/olj.v23i3.1546>
- Gorelick, N., Hancher, M., Dixon, M., Ilyushchenko, S., Thau, D., & Moore, R. (2017). Google Earth Engine: Planetary-scale geospatial analysis for everyone. *Remote Sensing of Environment*, *202*, 18–27. <https://doi.org/10.1016/j.rse.2017.06.031>
- Herndon, E. M., Yang, Z., Bargar, J., Janot, N., Regier, T. Z., Graham, D. E., et al. (2015). Geochemical drivers of organic matter decomposition in arctic tundra soils. *Biogeochemistry*, *126*(3), 397–414. <https://doi.org/10.1007/s10533-015-0165-5>
- Hirst, C., Andersson, P. S., Shaw, S., Burke, I. T., Kutscher, L., Murphy, M. J., et al. (2017). Characterisation of Fe-bearing particles and colloids in the Lena River basin, NE Russia. *Geochimica et Cosmochimica Acta*, *213*, 553–573. <https://doi.org/10.1016/j.gca.2017.07.012>
- Ilna, S. M., Poitrasson, F., Lapitskiy, S. A., Alekhin, Y. V., Viers, J., & Pokrovsky, O. S. (2013). Extreme iron isotope fractionation between colloids and particles of boreal and temperate organic-rich waters. *Geochimica et Cosmochimica Acta*, *101*, 96–111. <https://doi.org/10.1016/j.gca.2012.10.023>
- Ingrí, J., Conrad, S., Lidman, F., Nordblad, F., Engström, E., Rodushkin, I., & Porcelli, D. (2018). Iron isotope pathways in the boreal landscape: Role of the riparian zone. *Geochimica et Cosmochimica Acta*, *239*, 49–60. <https://doi.org/10.1016/j.gca.2018.07.030>
- Ingrí, J., Malinovsky, D., Rodushkin, I., Baxter, D. C., Widerlund, A., Andersson, P., et al. (2006). Iron isotope fractionation in river colloidal matter. *Earth and Planetary Science Letters*, *245*(3–4), 792–798. <https://doi.org/10.1016/j.epsl.2006.03.031>
- Jessen, S., Holmslykke, H. D., Rasmussen, K., Richardt, N., & Holm, P. E. (2014). Hydrology and pore water chemistry in a permafrost wetland, Ilulissat, Greenland. *Water Resources Research*, *50*(6), 4760–4774. <https://doi.org/10.1002/2013WR014376>
- Kalbitz, K., Schmerwitz, J., Schwesig, D., & Matzner, E. (2003). Biodegradation of soil-derived dissolved organic matter as related to its properties. *Geoderma*, *113*(3–4), 273–291. [https://doi.org/10.1016/S0016-7061\(02\)00365-8](https://doi.org/10.1016/S0016-7061(02)00365-8)
- Kawahigashi, M., Kaiser, K., Kalbitz, K., Rodionov, A., & Guggenberger, G. (2004). Dissolved organic matter in small streams along a gradient from discontinuous to continuous permafrost. *Global Change Biology*, *10*(9), 1576–1586. <https://doi.org/10.1111/j.1365-2486.2004.00827.x>
- Krachler, R., & Krachler, R. F. (2021). Northern high-latitude organic soils as a vital source of river-borne dissolved iron to the ocean. *Environmental Science and Technology*, *55*(14), 9672–9690. <https://doi.org/10.1021/acs.est.1c01439>
- Krachler, R., Krachler, R. F., Wallner, G., Steier, P., El Abiead, Y., Wiesinger, H., et al. (2016). Sphagnum-dominated bog systems are highly effective yet variable sources of bio-available iron to marine waters. *Science of the Total Environment*, *556*, 53–62. <https://doi.org/10.1016/j.scitotenv.2016.03.012>
- Laglera, L. M., & Vandenbergh, C. M. G. (2009). Evidence for geochemical control of iron by humic substances in seawater. *Limnology and Oceanography*, *54*(2), 610–619. <https://doi.org/10.4319/lo.2009.54.2.0610>
- Landre, A. L., Watmough, S. A., & Dillon, P. J. (2009). The effects of dissolved organic carbon, acidity and seasonality on metal geochemistry within a forested catchment on the Precambrian Shield, central Ontario, Canada. *Biogeochemistry*, *93*(3), 271–289. <https://doi.org/10.1007/s10533-009-9305-0>
- Levshina, S. I. (2012). Iron distribution in surface waters in the Middle and Lower Amur basin. *Water Resources*, *39*(4), 375–383. <https://doi.org/10.1134/s0097807812040082>
- Martin, J. H., Coale, K. H., Johnson, K. S., Fitzwater, S. E., Gordon, R. M., Tanner, S. J., et al. (1994). Testing the iron hypothesis in ecosystems of the equatorial Pacific Ocean. *Nature*, *371*(6493), 123–129. <https://doi.org/10.1038/371123a0>
- Martin, J. H., & Fitzwater, S. E. (1988). Iron deficiency limits phytoplankton growth in the North-East Pacific subarctic. *Nature*, *336*(6154), 403–405. <https://doi.org/10.1038/331341a0>
- Martin, J. H., Gordon, R., & Fitzwater, S. E. (1990). Iron in Antarctic waters. *Nature*, *345*(6271), 156–158. <https://doi.org/10.1038/345156a0>
- Martin, J. H., Gordon, R. M., Fitzwater, S. E., & Broenkow, W. W. (1989). Vertex: Phytoplankton/iron studies in the Gulf of Alaska. *Deep Sea Research Part A*, *36*(5), 649–680. [https://doi.org/10.1016/0198-0149\(89\)90144-1](https://doi.org/10.1016/0198-0149(89)90144-1)
- Matsunaga, K., Nishioka, J., Kuma, K., Toya, K., & Suzuki, Y. (1998). Riverine input of bioavailable iron supporting phytoplankton growth in Kesennuma Bay (Japan). *Water Research*, *32*(11), 3436–3442. [https://doi.org/10.1016/S0043-1354\(98\)00113-4](https://doi.org/10.1016/S0043-1354(98)00113-4)

- Moore, J. K., & Braucher, O. (2008). Sedimentary and mineral dust sources of dissolved iron to the world ocean. *Biogeosciences*, 5(3), 631–656. <https://doi.org/10.5194/bg-5-631-2008>
- Nagao, S., Motoki, T., Kodama, H., Kim, V. I., Shesterkin, P. V., & Makhinov, A. N. (2007). Migration behaviour of Fe in the Amur River Basin. In T. Shiraiwa (Ed.), *Report on Amur - Okhotsk project No. 4* (pp. 37–48). Research Institute for Humanity and Nature. Retrieved from <http://id.nii.ac.jp/1422/00002607/>
- Neubauer, E., Köhler, S. J., Von Der Kammer, F., Laudon, H., & Hofmann, T. (2013). Effect of pH and stream order on iron and arsenic speciation in boreal catchments. *Environmental Science and Technology*, 47(13), 7120–7128. <https://doi.org/10.1021/es401193j>
- Nishioka, J., Nakatsuka, T., Ono, K., Volkov, Y. N., Scherbinin, A., & Shiraiwa, T. (2014). Quantitative evaluation of iron transport processes in the Sea of Okhotsk. *Progress in Oceanography*, 126, 180–193. <https://doi.org/10.1016/j.pocean.2014.04.011>
- Obu, J., Westermann, S., Bartsch, A., Berdnikov, N., Christiansen, H. H., Dashtseren, A., et al. (2019). Northern hemisphere permafrost map based on TTOP modelling for 2000–2016 at 1 km² scale. *Earth-Science Reviews*, 193, 299–316. <https://doi.org/10.1016/j.earscirev.2019.04.023>
- Olefeldt, D., Persson, A., & Turetsky, M. R. (2014). Influence of the permafrost boundary on dissolved organic matter characteristics in rivers within the Boreal and Taiga plains of western Canada. *Environmental Research Letters*, 9(3), 035005. <https://doi.org/10.1088/1748-9326/9/3/035005>
- Olefeldt, D., Roulet, N., Giesler, R., & Persson, A. (2013). Total waterborne carbon export and DOC composition from ten nested subarctic peatland catchments—importance of peatland cover, groundwater influence, and inter-annual variability of precipitation patterns. *Hydrological Processes*, 27(16), 2280–2294. <https://doi.org/10.1002/hyp.9358>
- Palviainen, M., Lehtoranta, J., Ekholm, P., Ruoho-airola, T., & Kortelainen, P. (2015). Land cover controls the export of terminal electron acceptors from boreal catchments. *Ecosystems*, 18(2), 343–358. <https://doi.org/10.1007/s10021-014-9832-y>
- Pan, X. F., Yan, B. X., & Muneoki, Y. (2011). Effects of land use and changes in cover on the transformation and transportation of iron: A case study of the Sanjiang Plain, Northeast China. *Science China Earth Sciences*, 54(5), 686–693. <https://doi.org/10.1007/s11430-010-4082-0>
- Petrone, K. C., Jones, J. B., Hinzman, L. D., & Boone, R. D. (2006). Seasonal export of carbon, nitrogen, and major solutes from Alaskan catchments with discontinuous permafrost. *Journal of Geophysical Research*, 111(2), 1–13. <https://doi.org/10.1029/2005JG000055>
- Pokrovsky, O. S., Dupré, B., & Schott, J. (2005). Fe-Al-organic colloids control of trace elements in peat soil solutions: Results of ultrafiltration and dialysis. *Aquatic Geochemistry*, 11(3), 241–278. <https://doi.org/10.1007/s10498-004-4765-2>
- Pokrovsky, O. S., Manasyrov, R. M., Loiko, S., Shirokova, L. S., Krickov, I. A., Pokrovsky, B. G., et al. (2015). Permafrost coverage, watershed area and season control of dissolved carbon and major elements in western Siberian rivers. *Biogeosciences*, 12(21), 6301–6320. <https://doi.org/10.5194/bg-12-6301-2015>
- Pokrovsky, O. S., Manasyrov, R. M., Loiko, S. V., Krickov, I. A., Kopysov, S. G., Kolesnichenko, L. G., et al. (2016). Trace element transport in western Siberian rivers across a permafrost gradient. *Biogeosciences*, 13(6), 1877–1900. <https://doi.org/10.5194/bg-13-1877-2016>
- Price, N. M., Ahner, B. A., & Morel, F. M. M. (1994). The equatorial Pacific Ocean: Grazer-controlled phytoplankton populations in an iron-limited ecosystem. *Limnology and Oceanography*, 39(3), 520–534. <https://doi.org/10.4319/lo.1994.39.3.0520>
- Russian International Technical Standards. (2006). Mass concentration of iron in water. Method of measurement by photometric method with 1-10, phenanthroline (RD52.24.358-2006). (In Russian). Retrieved from <https://files.stroyinf.ru/Index2/1/4293837/4293837319.htm>
- Sarkkola, S., Nieminen, M., Koivusalo, H., Laurén, A., Kortelainen, P., Mattsson, T., et al. (2013). Iron concentrations are increasing in surface waters from forested headwater catchments in eastern Finland. *Science of the Total Environment*, 463–464, 683–689. <https://doi.org/10.1016/j.scitotenv.2013.06.072>
- Shamov, V. V., Onishi, T., & Kulakov, V. V. (2014). Dissolved iron runoff in Amur Basin Rivers in the late XX century. *Water Resources*, 41(2), 201–209. <https://doi.org/10.1134/S0097807814020122>
- Shiraiwa, T. (2012). “Giant Fish-Breeding Forest”: A new environmental system linking continental watershed with open water. In M. Taniguchi & T. Shiraiwa (Eds.), *The dilemma of boundaries* (pp. 73–85). Springer. https://doi.org/10.1007/978-4-431-54035-9_8
- Sorokin, Y. I., & Sorokin, P. Y. (1999). Production in the Sea of Okhotsk. *Journal of Plankton Research*, 21(2), 201–230. <https://doi.org/10.1093/plankt/21.2.201>
- Spencer, R. G. M., Aiken, G. R., Wickland, K. P., Striegl, R. G., & Hernes, P. J. (2008). Seasonal and spatial variability in dissolved organic matter quantity and composition from the Yukon River basin, Alaska. *Global Biogeochemical Cycles*, 22(4), 1–13. <https://doi.org/10.1029/2008GB003231>
- Sunda, W. G. (2012). Feedback interactions between trace metal nutrients and phytoplankton in the ocean. *Frontiers in Microbiology*, 3, 204. <https://doi.org/10.3389/fmicb.2012.00204>
- Suzuki, K., Hattori-Saito, A., Sekiguchi, Y., Nishioka, J., Shigemitsu, M., Isada, T., et al. (2014). Spatial variability in iron nutritional status of large diatoms in the Sea of Okhotsk with special reference to the Amur River discharge. *Biogeosciences*, 11(9), 2503–2517. <https://doi.org/10.5194/bg-11-2503-2014>
- Takeda, S., & Obata, H. (1995). Response of equatorial Pacific phytoplankton to subnanomolar Fe enrichment. *Marine Chemistry*, 50(1–4), 219–227. [https://doi.org/10.1016/0304-4203\(95\)00037-R](https://doi.org/10.1016/0304-4203(95)00037-R)
- Takeuchi, W., & Yasuoka, Y. (2004). Development of normalized vegetation, soil and water indices derived from satellite remote sensing data. *Journal of the Japan Society of Photogrammetry and Remote Sensing*, 43(6), 7–19. (In Japanese). https://doi.org/10.4287/jsp.43.6_7
- Tashiro, Y., Yoh, M., Shesterkin, V., Shiraiwa, T., Onishi, T., & Kim, V. (2023). Dataset of water chemistry and land and soil characteristics in the Tyrma region [Dataset]. Figshare. <https://doi.org/10.6084/m9.figshare.23735487.v1>
- Tashiro, Y., Yoh, M., Shiraiwa, T., Onishi, T., Shesterkin, V., & Kim, V. (2020). Seasonal variations of dissolved iron concentration in active layer and rivers in permafrost areas, Russian Far East. *Water*, 12(9), 2579. <https://doi.org/10.3390/w12092579>
- Tipping, E. (Ed.). (2002). *Cation binding by humic substances*, Cambridge Environmental Chemistry Series. Cambridge University Press. <https://doi.org/10.1017/CBO9780511535598>
- Tucker, C. J., Townshend, J. R. G., & Goff, T. E. (1985). African land-cover classification using satellite data. *Science*, 227(4685), 369–375. <https://doi.org/10.1126/science.227.4685.369>
- Vorobyev, S. N., Pokrovsky, O. S., Serikova, S., Manasyrov, R. M., Krickov, I. V., Shirokova, L. S., et al. (2017). Permafrost boundary shift in Western Siberia may not modify dissolved nutrient concentrations in rivers. *Water*, 9(12), 985. <https://doi.org/10.3390/w9120985>
- Wang, L., Yan, B., Pan, X., & Zhu, H. (2012). The spatial variation and factors controlling the concentration of total dissolved iron in rivers, Sanjiang Plain. *Clean – Soil, Air, Water*, 40(7), 712–717. <https://doi.org/10.1002/clen.201100251>